Title:

Estimation of identification limit for a small-type OSL dosimeter on the medical images by measurement of X-ray spectra

Authors:

Kazuki Takegami[1),*], Hiroaki Hayashi[2),#], Hiroki Okino[1)], Natsumi Kimoto[1)], Itsumi Maehata[3)], Yuki Kanazawa[2)], Tohru Okazaki[4)], Takuya Hashizume[4)], Ikuo Kobayashi[4)]

1) Graduate School of Health Sciences, Tokushima University
3-18-15 Kuramoto-cho, Tokushima, Tokushima 770-8503, Japan

2) Graduate school of Biomedical Sciences, Tokushima University
3-18-15 Kuramoto-cho, Tokushima, Tokushima 770-8503, Japan

3) School of Health Sciences, Tokushima University
3-18-15 Kuramoto-cho, Tokushima, Tokushima 770-8503, Japan

4) Nagase Landauer, LTD.
C22-1 Suwa, Tsukuba, Ibaraki 300-2686, Japan

Corresponding Author:
Hiroaki HAYASHI
Institute of Biomedical Sciences, Tokushima University Graduate School
3-18-5 Kuramoto-cho, Tokushima, Tokushima 770-8503, Japan
+81-88-633-9054
hayashi.hiroaki@tokushima-u.ac.jp

*Present Affiliation
Kazuki Takegami
Yamaguchi University Hospital
1-1-1 MinamiKogushi, Ube,Yamaguchi 755-8505, Japan

Keywords: OSL dosimeter; CdTe detector; Patient exposure dose measurement; Diagnostic X-rays

Abstract:

Our aim in this study is to derive an identification limit on a dosimeter for not disturbing a medical image when patients wear a small-type optically stimulated luminescence (OSL) dosimeter on their bodies during X-ray diagnostic imaging. For evaluation of the detection limit based on an analysis of X-ray spectra, we propose a new quantitative identification method. We performed experiments for which we used diagnostic X-ray equipment, a soft-tissue-equivalent phantom (1–20 cm), and a CdTe X-ray spectrometer assuming one pixel of the X-ray imaging detector. Then, with the following two experimental settings, corresponding X-ray spectra were measured with 40–120 kVp and 0.5–1000 mAs at a source-to-detector distance of 100 cm: 1) X-rays penetrating a soft-tissue-equivalent phantom with the OSL dosimeter attached directly on the phantom, and 2) X-rays penetrating only the soft-tissue-equivalent phantom. Next, the energy fluence and errors in the fluence were calculated from the spectra. When the energy fluence with errors concerning these two experimental conditions were estimated to be indistinctive, we defined the condition as the OSL dosimeter not being identified on the X-ray image. Based on our analysis,

we determined the identification limit of the dosimeter. We then compared our results with those for the general irradiation conditions used in clinics. We found that the OSL dosimeter could not be identified under the irradiation conditions of abdominal and chest radiography; namely, one can apply the OSL dosimeter to measurement of the exposure dose in the irradiation field of X-rays without disturbing medical images.

1 Introduction

X-ray examinations are generally used as simple and quick methods for detecting diseases. For early detection and proper diagnosis, the image quality is a key factor. In recent years, precise examinations based on high-quality images have been required. However, medical X-ray exposure to patients was considered to be one of the causes of carcinogenesis [1]. There is a trade-off between image quality and patient dose; therefore, finding a proper balance and optimizing the X-ray exposure for each examination are important [2].

The exposure dose to the medical staff is generally measured with personal dosimeters such as optically stimulated luminescence (OSL) dosimeters, glass dosimeters [3], and thermoluminescence dosimeters (TLDs) [4,5], which are attached to the body. For measurement of the patient exposure dose, it is, however, difficult to use these dosimeters, because they interfere with medical images. For proper management of the patient exposure dose, the development of a dosimeter which does not interfere with the medical images is desired.

Recently, a small-type OSL dosimeter, named “nanoDot”, was made commercially available by Landauer, Inc., and this was applied to the measurement of the absorbed dose during radiotherapy [6-9]. We consider that the nanoDot OSL dosimeter can measure the exposure dose of patients in the diagnostic X-ray region; this dosimeter is small (10 mm width, 10 mm length, and 2 mm thickness); therefore, it is wearable without distraction from an X-ray examination. We have previously reported on basic research on the nanoDot OSL dosimeter: on the methodology for converting the measured value to exposure dose [10,11], angular dependence [12,13], energy dependence [14], initialization method for the dosimeter [15], and a high-accuracy measurement method [16]. According to our findings, it is expected that the nanoDot OSL dosimeter can directly measure the patient exposure dose. By showing evidence that this dosimeter does not interfere with medical images, our research will lead to progress toward its clinical application.

In our previous reports [11,16], a visual evaluation of the nanoDot OSL dosimeter as to whether it is identified on the X-ray image was carried out. In simple demonstrations by means of radiographs of body phantoms, it seemed that the nanoDot OSL dosimeter was not observed on X-ray images.

On the other hand, a quantitative evaluation has not been published. In the present study, we proposed a new quantitative identification method from the point of view of material identification based on X-ray spectrum measurements.

2 Materials and methods

2.1 Experiment

Fig.1

Figure 1 shows schematic drawings of experimental settings. Incident X-rays were produced with general diagnostic X-ray equipment **(TOSHIBA Medical Systems Corporation, Nasu, Japan)**. A CdTe detector **(EMF-123 type, EMF Japan Co., Ltd., Osaka, Japan)** was used for measurements of X-ray spectra. The distance between the CdTe detector and the X-ray source was 100 cm. For reduction of scattered X-rays **[17]** generated by air, the surrounding materials, and a movable diaphragm as part of the X-ray equipment, a tungsten collimator having a hole 0.2 mm in diameter was set in front of the CdTe detector. That size is similar to the one-pixel size used for X-ray detectors of medical imaging such as in computed

Table.1

radiography (CR) systems, digital radiography (DR) systems, etc.; namely, an area of the hole 0.2 mm in diameter is equivalent to that of a square having 0.177 mm in side. To find the identification limit for the small-type OSL nanoDot dosimeter **(Landauer Corporation, Glenwood, Illinois, USA)**, we carried out spectrum measurements under the following two experimental conditions: In **Fig.1(a)**, the CdTe detector measures X-rays penetrating both a soft-tissue-equivalent phantom **(Kyoto Kagaku Co., Ltd., Kyoto, Japan)** and the nanoDot OSL dosimeter which is attached to the front of the phantom; and in **Fig.1(b)**, the CdTe detector detects X-rays penetrating the phantom only. The experiments were performed under the following irradiation conditions summarized in **Table 1**; phantom thicknesses were 1, 5, 10, and 20 cm; tube voltages were 40, 60, 80, and 120 kVp; and tube current-time products were 0.5-1000 mAs. The currents (mA values) were determined so as to provide a proper counting rate (less than 10 kilo-counts per second) for the CdTe detector, and the effects of pile-up and dead time **[18-20]** were negligibly small for the experimental conditions. The spectra measured with the CdTe detector were unfolded with response functions derived by a Monte-Carlo simulation code (electron gamma shower ver. 5: EGS5) **[21, 22]**.

2.2 Analysis and proposed identification method

We will explain our quantitative identification method with the use of X-ray spectra which were the same as the unfolded spectra in the experiments. In the realistic X-ray detector, the absorbed energy contributes an image density (pixel value). Then, the absorbed energy for an X-ray having an energy E can be estimated by $\Phi(E) \times E \times \varepsilon$, where $\Phi(E)$ and ε are the fluence and the detection efficiency of the X-ray detector, respectively. In the present study, we assumed an ideal X-ray detector having ε=1.0 for all energies. Therefore, the image density can be estimated as the integration value of $\Phi(E) \times E$ for all energies. The integration value is known as the energy fluence "Ψ":

$$\Psi = \int \Phi(E) \times EdE. \tag{1}$$

According to the Poisson distribution, a certain energy bin in the spectrum $\Phi(E)$ has statistical fluctuation, and the value of the fluctuation is theoretically derived by the square root of $\Phi(E)$. Then, with use of an error propagation formula [21], the error "σ" of Ψ is derived in the following equation:

$$\sigma = \sqrt{\int \left(\mathrm{E} \times \sqrt{\Phi(\mathrm{E})}\right)^2 \mathrm{dE}}. \qquad (2)$$

Basically, Ψ of the experiment in **Fig.1 (a)**, $\Psi_{\mathrm{Phantom+OSL}}$, should have a smaller value than that of the experiment in **Fig.1 (b)**, Ψ_{Phantom}, but because of uncertainties σs, there are cases in which one cannot distinguish between $\Psi_{\mathrm{Phantom+OSL}} \pm \sigma$ and $\Psi_{\mathrm{Phantom}} \pm \sigma$. When we cannot distinguish the difference between $\Psi_{\mathrm{Phantom+OSL}} \pm \sigma$ and $\Psi_{\mathrm{Phantom}} \pm \sigma$, this means that the nanoDot OSL dosimeter may not be identified in a medical image. Therefore, we compared the difference between $\Psi_{\mathrm{Phantom+OSL}} \pm \sigma$ and $\Psi_{\mathrm{Phantom}} \pm \sigma$.

Here, the smallest limit of $\Psi_{\mathrm{Phantom+OSL}} \pm \sigma$, namely $\{\Psi - \sigma\}_{Phantom}$, is compared with the largest limit, $\{\Psi + \sigma\}_{Phantom+OSL}$. We then define the following criteria for identification of the nanoDot OSL dosimeter on the one pixel of the ideal imaging detector:

Identified: $\{\Psi - \sigma\}_{Phantom} - \{\Psi + \sigma\}_{Phantom+OSL} > 0$, (3)

Not identified: $\{\Psi - \sigma\}_{Phantom} - \{\Psi + \sigma\}_{Phantom+OSL} < 0$. (4)

As the exposure dose increases, the absolute values of Ψ and σ become larger, and the relative value of σ/Ψ becomes smaller. This means that the equations (3) and (4) are functions of the exposure dose, which is proportional to the tube current-time product (mAs) of the X-ray equipment. So, we determine the following boundary condition as a function of the mAs value:

Boundary condition: $\{\Psi - \sigma\}_{Phantom}(\mathrm{mAs}) = \{\Psi + \sigma\}_{Phantom+OSL}(\mathrm{mAs})$. (5)

In the actual case of our analysis, we obtained the tube current-time product corresponding to the boundary condition of equation (5). The measured data for Ψ are affected by statistical fluctuations. In order to reduce the effect of statistical fluctuations on the measured Ψ, we evaluated the most provable value of Ψ. By use of all of the experimental data for each examination setup, a plot of Ψ versus mAs values was made, and the curve was fitted by use of a linear function. In this fitting, the least square method with weights of $1/\sigma^2$ was applied **[23]**. Then, we used Ψ derived from the fitted function for equation (5) instead of the experimental value of Ψ.

3 Results

Fig.2

Figure 2 shows the typical spectra measured with the two experimental protocols (see **Fig.1** (a) and (b)). The tube current-time products of the spectra in **Fig. 2** (a) and (b) were 10 and 100 mAs, respectively. The horizontal axis indicates the energy “E [keV]” which was calibrated precisely to be 0.2 keV/channel **[24]**. The vertical axis indicates the counts corresponding to the energy bin of 0.2 keV. Here, the counts were divided by the cross-section of the collimator, 3×10^{-4} cm^2, for converting a dimension (value) so that it agreed with that of the fluence. Then, the energy fluence

Fig.3

"Ψ" and the error "σ" were derived based on equations (1) and (2). For example, in the case of a 10 mAs X-ray irradiation as shown in **Fig. 2 (a)**, the following calculated results were obtained; $(\Psi \pm \sigma)_{\mathrm{Phnatom+OSL}}$ was 73949 ± 1814 [keV/cm^2], and $(\Psi \pm \sigma)_{\mathrm{Phnatom}}$ was 76789 ± 1849 [keV/cm^2]. In this condition of 10 mAs, the nanoDot OSL dosimeter located on the phantom cannot be identified because "$(\Psi + \sigma)_{\mathrm{Phnatom+OSL}} = 73949 + 1814 = 75763$" is larger than "$(\Psi - \sigma)_{\mathrm{Phnatom}} = 76789 - 1849 = 74940$" (equation (3) is applied). In the same manner, the above mentioned analysis was applied to all experimental spectra, and we evaluated whether the nanoDot OSL dosimeter could be identified.

Figure 3 shows the relationship between energy fluence and irradiation dose for the conditions of tube voltage 60 kVp and phantom thickness 15 cm. The open circles represent the energy fluence derived in the experiment of **Fig. 1 (a)**, and the closed circles represent those in the experiment of **Fig. 1**

(b). Close-up views corresponding to 10, 16.7, and 100 mAs show relationships of the results concerning two experimental settings for the typical three conditions of “not identified”, “boundary”, and “identified”, respectively. It is clearly seen that the high mAs values are capable of identifying the nanoDot OSL dosimeter. The boundary doses are summarized in **Table 2**.

Table2

Fig.4

Figure 4 (a), (b), (c), and **(d)** show two-dimensional maps for displaying the usable irradiation conditions for tube voltages of 40, 60, 80, and 120 kVp, respectively. The horizontal axis shows the phantom thickness, and the vertical axis shows the tube current-time product concerning the irradiation dose (mAs value). The closed triangles indicate the boundary conditions which are summarized in **Table 2**. The usable conditions (i.e., nanoDot is unobservable) are indicated by shaded portions in the graphs.

4 Discussion

In this study, we clarified the boundary dose at which the small-type OSL dosimeter, named nanoDot, does not interfere with a medical image.

This study provides evidence that the nanoDot OSL dosimeter can be applied to the measurement of exposure dose to patients during clinical X-ray examinations. In addition to the previous report on visual demonstrations of the nanoDot OSL dosimeter **[11,16]**, the present result gives valuable evidence for its lack of visibility. In this paper, we used a novel method to verify the invisibility of the nanoDot OSL dosimeter. We describe the reason as follows. For example, if we use a computed radiography system as an X-ray imaging detector, the results strongly depend on the CR system used. On the other hand, the present results were led by the X-ray spectra which were fundamental information for X-ray imaging detector, therefore these results can be commonly applied to all X-ray imaging detectors. In the following, we discuss the proper irradiation conditions for applying the nanoDot OSL dosimeter in clinical settings, and the limitations of our experiments.

In **Fig. 4**, we present a two-dimensional map of the boundary doses as a function of the phantom thickness. Here, our results were compared with the radiography conditions, in which mean values of tube voltage and thickness of the photographic object were studied based on a survey in Japan

[25]. The black circles in **Fig. 4** show the averaged conditions. The conditions included various source-to-image distances (SIDs); therefore, the mAs values were corrected so as to be normalized to the distance of 100 cm by use of the formula for the inverse square of the distance. For example, a typical chest radiography condition is 5.5 mAs at SID=193 cm. The mAs value was corrected to 1.5 mAs (= 5.5 mAs $\times$ $(100/193)^2$). In the graph of **Fig. 4**, the chest radiography condition (tube voltage: 121 kVp, body thickness: 20 cm) was included in the shaded area of 120 kVp. The result indicates that the patient dose can be measured with the nanoDot OSL dosimeter without interfering with radiographic images for chest radiography. Note that the thickness (X axis) corresponds to that of the soft-tissue-equivalent material. The effective thickness of the lung field in the real chest radiography is considered to be less than 20 cm, because the field is composed of air and soft-tissue regions. On the other hand, the other parts of the chest X-ray image consist of organs, bones, and soft-tissue, and the soft-tissue-equivalent thickness is considered to be larger than 20 cm, because an attenuation factor of bone is larger than that of the soft-tissue. In the former case, the nanoDot OSL dosimeter should not be applied, and in the latter case, the dosimeter can be applied. In this manner, our method applying to chest radiographs should be cared. For other parts of radiography regions, we can simply state; the nanoDot OSL dosimeter may be applied to examinations of the abdomen (tube voltage: 79 kVp, body thickness: 20 cm) and for the chest of babies (tube voltage: 66 kVp, body thickness: 10 cm). In contrast for radiography of the ankle (tube voltage: 52 kVp, body thickness: 7 cm), we cannot evaluate the result clearly at this time. For the general conditions for X-ray radiography of thin body parts such as the extremities, there is the possibility that the nanoDot OSL dosimeter will interfere with X-ray images. In the next paragraph, we discuss a potential application of the direct dose measurement using the nanoDot OSL dosimeter for clinical use.

In our experiments, we used a soft-tissue-equivalent phantom instead of the actual human body. In reality, the human body consists of complicated compositions of bones, various organs, water, etc., which have different densities and atomic compositions from that of soft-tissue. The soft-tissue material is composed of relatively light atoms compared with other materials in the structure of the human body. Therefore, our experimental conditions should be considered carefully; when a photographic object has relatively high-atomic-number materials, the nanoDot OSL dosimeter is less observable. Our results indicated in **Fig. 4** should be evaluated with prudence.

Our method is based on the point of view of the identification of a substance with the help of the X-ray spectrum; namely, the experiment can evaluate the effect for certain one pixel in the two-dimensional imaging detector. At this time, it is not clear when a two-dimensional image (medical image) was used for evaluation of the invisibility of the nanoDot OSL dosimeter from an analysis of observation, especially for observation by experts of X-ray examinations. We consider that receiver operating characteristic curve (ROC) analysis will also provide a valuable evidence in addition to the present experiment.

5 Conclusion

In the present study, we investigated the visibility of a small-type OSL dosimeter on medical images. Based on the variations in the measured counts of the spectra measured with a CdTe detector, we determined the identification boundary dose at which the nanoDot OSL dosimeter does not interfere with a medical image. We also constructed a graph that indicates the range of irradiation conditions in which the nanoDot OSL dosimeter is not observable. The general irradiation conditions used in clinics were also evaluated. Then, we estimated that the nanoDot OSL dosimeter may not be observable in the chest and abdominal images. In particular, it was clarified that the nanoDot OSL dosimeter can be applied directly to measurement of the patient dose without interfering with medical images.

Acknowledgment:

This work was supported by JSPS KAKENHI Grant Number 15K19205.

Conflict of interest:

T. Okazaki, T. Hashizume, and I. Kobayashi are employees of Nagase Landauer Ltd. and are collaborative researchers.

References:

[1] Amy Berrington de Gonzalez and Sarah Darby. Risk of cancer from diagnostic X-ray: estimates for the UK and 14 other countries, The Lancet. 2004;363:345-351. (doi: org/10.1016/S0140-6736(04)15433-0)

[2] Uffmann M, Prokop CS. Digital radiography: The balance between image quality and required radiation dose, Eur. J. Radiol. 2009;72:202-208. (doi: 10.1016/j.ejrad.2009.05.060)

[3] Komiya I, Shirasaka T, Umezu Y, et al. Patient Dose Measurement with Fluorescent Glass Dosimeter: Characteristics Evaluation and Patient Skin Dose Measurement in Abdominal Interventional Radiology, Jpn. J. Radiol. Technol. 2003;60(2):270-277.

[4] Shortt CP, Malone L, Thornton J, et al. Radiation protection to the eye and thyroid suring diagnostic cerebral angiogralhy: A phantom study, J. Med. Imaging Radiat. Oncol. 2008;52:365-369. (doi: 10.1111/j.1440-1673.2008.01970.x)

[5] Matsunaga Y, Kawaguchi A, Kobayashi K, et al. Dose Estimation for Exposure Conditions of Diagnostic Radiology Acquired by a 2011 Questionnaire in a Phantom Study. Jpn. J. Radiol. Technol.

2013;69(12):1372-1378. (doi: org/10.6009/jjrt.2013_JSRT_69.12.1372)

[6] Jursinic PA. Characterization of optically stimulated luminescent dosimeters, OSLDs, for clinical dosimetric measurements, Med. Phys. 2007;34(12):4594-4604. (doi: 10.1118/1.2804555)

[7] Reft CS. The energy dependence and dose response of a commercial optically stimulated luminescent detector for kilovoltage photon, megavoltage photon, and electron, proton, and carbon beams, Med. Phys. 2009;36(5):1690-1699. (doi: 10.1118/1.3097283)

[8] Lehmann J, Dunn L, Lye JE, et al. Angular dependence of the response of the nanoDot OSLD system for measurements at depth in clinical megavoltage beams, Med. Phys. 2014;41(6):061712-1-9, 2014. (doi: org/10.1118/1.4875698)

[9] Kerns JR, Kry SF, Sahoo N, et al. Angular dependence of the nanoDot OSL dosimeter, Med. Phys. 2011;38(7):3955-3962. (doi: org/10.1118/1.3596533)

[10] Takegami K, Hayashi H, Okino H, et al. Practical calibration curve of small-type optically stimulated luminescence (OSL) dosimeter for evaluation of entrance-skin dose in the diagnostic X-ray, Radiol. Phys. Technol. 2015;8:286-294. (doi: 10.1007/s12194-015-0318-1)

[11] Takegami K, Hayashi H, Nakagawa K, et al. Measurement method of an exposed dose using the nanoDot dosimeter, Eur. Sor. Radiol. (EPOS). 2015. (doi:10.1594/ecr2015/C-0218)

[12] Hayashi H, Takegami K, Okino H, et al. Procedure to measure angular dependences of personal dosimeters by means of diagnostic X-ray equipment, Med. Imaging Inf. Sci. 2015;32(1):8-14. (doi: 10.11318/mii.32.8)

[13] Okazaki T, Hayashi H, Takegami K, et al. Evaluation of angular dependence of nanoDot OSL dosimeters toward direct measurement of entrance skin dose, Eur. Soc. Radiol. (EPOS). 2015. (doi: 10.1594/ecr2015/C-0721)

[14] Takegami K, Hayashi H, Okino H, et al. Energy dependence measurement of small-type optically stimulated luminescence (OSL) dosimeter by means of characteristic X-rays induced with general diagnostic X-ray equipment, Radiol. Phys. Technol. 2015. (doi: 10.1007/s12194-015-0339-9) (in press)

[15] Nakagawa N, Hayashi H, Okino H, et al. Fabrication of Annealing Equipment for Optically Stimulated Luminescence (OSL) Dosimeter, Jpn. J. Radiol. Technol. 2014;70(10):1135-1142. (doi:

10.6009/jjrt.2014_JSRT_70.10.1135)

[16] Hayashi H, Nakagawa K, Okino H, et al. High accuracy measurements by consecutive readings of OSL dosimeter, Med. Imaging Inf. Sci. 2014;31(2):28-34. (doi: 10.11318/mii.31.28)

[17] Maehata I, Hayashi H, Kimoto N. Practical method for determination of air-kerma by using an ionization chamber toward the construction of secondary X-ray field to be used in clinical examination rooms, Radiol. Phys. and Tech. (Accepted)

[18] Debertin K and Schötzig U. Limitations of the pulser method for pile-up corrections in Ge(Li)-spectrometry, Nucl. Instrum. Methods. 1977;140(2):337-340. (doi: 10.1016/0029-554X(77)90302-0)

[19] Then SS, Geurink FDP, Bode P. A pulse generator simulating Ge-detector signals for dead-time and pile-up correction in gamma-ray spectrometry in INAA without distortion of the detector spectrum, J. Radioanal. Nucl. Chem. 1997;215(2):249-252.(doi: 10.1007/BF02034473)

[20] Cano-Ott D, Tain JL, Gadea A. Pulse pileup correction of large NaI(Tl) total absorption spectra using the true pulse shape, Nucl. Instrum. Methods. 1999;430:488-497. (doi: 10.1016/S0168-9002(99)00216-8)

[21] Hirayama H, Namito Y, Bielajew AF, et al. The EGS5 code system, SLAC Report number: SLAC-R-730, KEK Report number: 2005-8.

[22] Okino H, Hayashi H, Nakagawa K, et al. Measurement of Response Function of CdTe Detector Using Diagnostic X-ray Equipment and Evaluation of Monte Carlo Simulation Code, Jpn. J. Radiol. Technol. 2014;70(12):1381-1391. (doi: 10.6009/jjrt.2014_JSRT_70.12.1381)

[23] Knoll GF. Radiation Detection and Measurement, New York: John Willy and Sons, Inc. 2000.

[24] Fukuda I, Hayashi H, Takegami K, et al. Development of an Experimental Apparatus for Energy Calibration of a CdTe Detector by Means of Diagnostic X-ray Equipment, Jpn. J. Radiol. Technol. 2013;69(9):952-959. (doi: 10.6009/jjrt.2013_JSRT_69.9.952)

[25] Asada Y, Suzuki S, Kobayashi K, et al. Summary of Results of the Patient Exposures in Diagnostic Radiography in 2011 Questionnaire -Focus on Radiographic Conditions-, Jpn. J. Radiol. Technol. 2012;69(9):1261-1268. (doi: 10.6009/jjrt.2012_JSRT_68.9.1261)

Figure captions:

Fig.1 Schematic drawing of experimental setup. A CdTe detector was used for measurement of X-ray spectra. In the experimental setup (a), X-rays that penetrated both the soft-tissue equivalent phantom and the nanoDot OSL dosimeter were measured. In experimental setup (b), X-rays that penetrated the phantom were measured. From the spectra obtained, the energy fluence and the error in the fluence were calculated.

Fig.2 Typical X-ray spectra measured with the CdTe detector. These spectra were unfolded with response functions. The spectra indicated by circles and lines show results for experiments (a) and (b) in **Fig. 1**, respectively.

Fig.3 Relationship between irradiation dose and energy fluence for experimental condition of 60 kVp for a phantom thickness of 15 cm. The insets show close-up views of experimental data and error bars for the two experimental setups.

Fig.4 Two-dimensional map for explanation of usable irradiation conditions in which the nanoDot OSL dosimeter cannot be identified. When the irradiation condition is in the shaded area for a certain X-ray examination, we can apply the nanoDot OSL dosimeter to measure exposure dose; in this condition, the nanoDot OSL dosimeter does not interfere with the medical images. The general irradiation conditions are also plotted as closed circles (see text).

Table 1 Irradiation conditions used.

Table 2 Summary of boundary conditions.

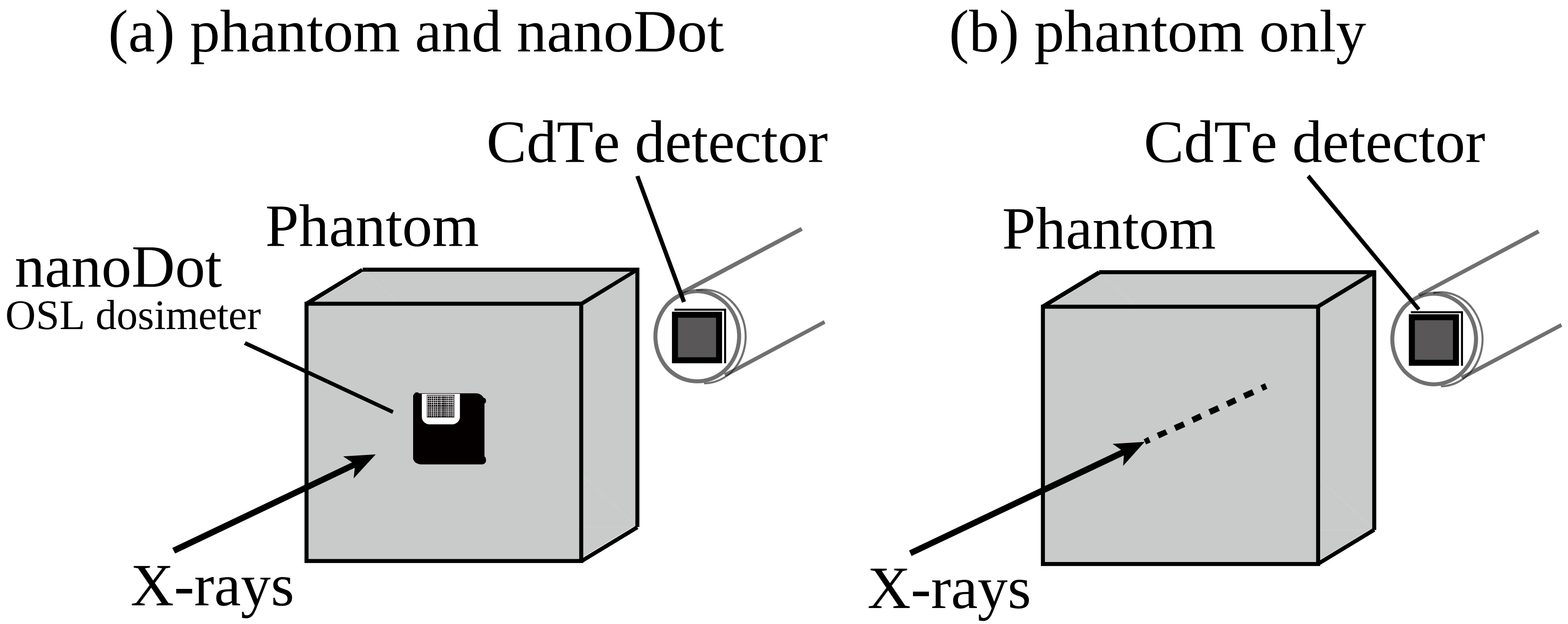
(a) phantom and nanoDot
(b) phantom only
CdTe detector
Phantom
nanoDot
OSL dosimeter
X-rays
CdTe detector
Phantom
X-rays

Fig.1

(a)10 mAs (b)100 mAs

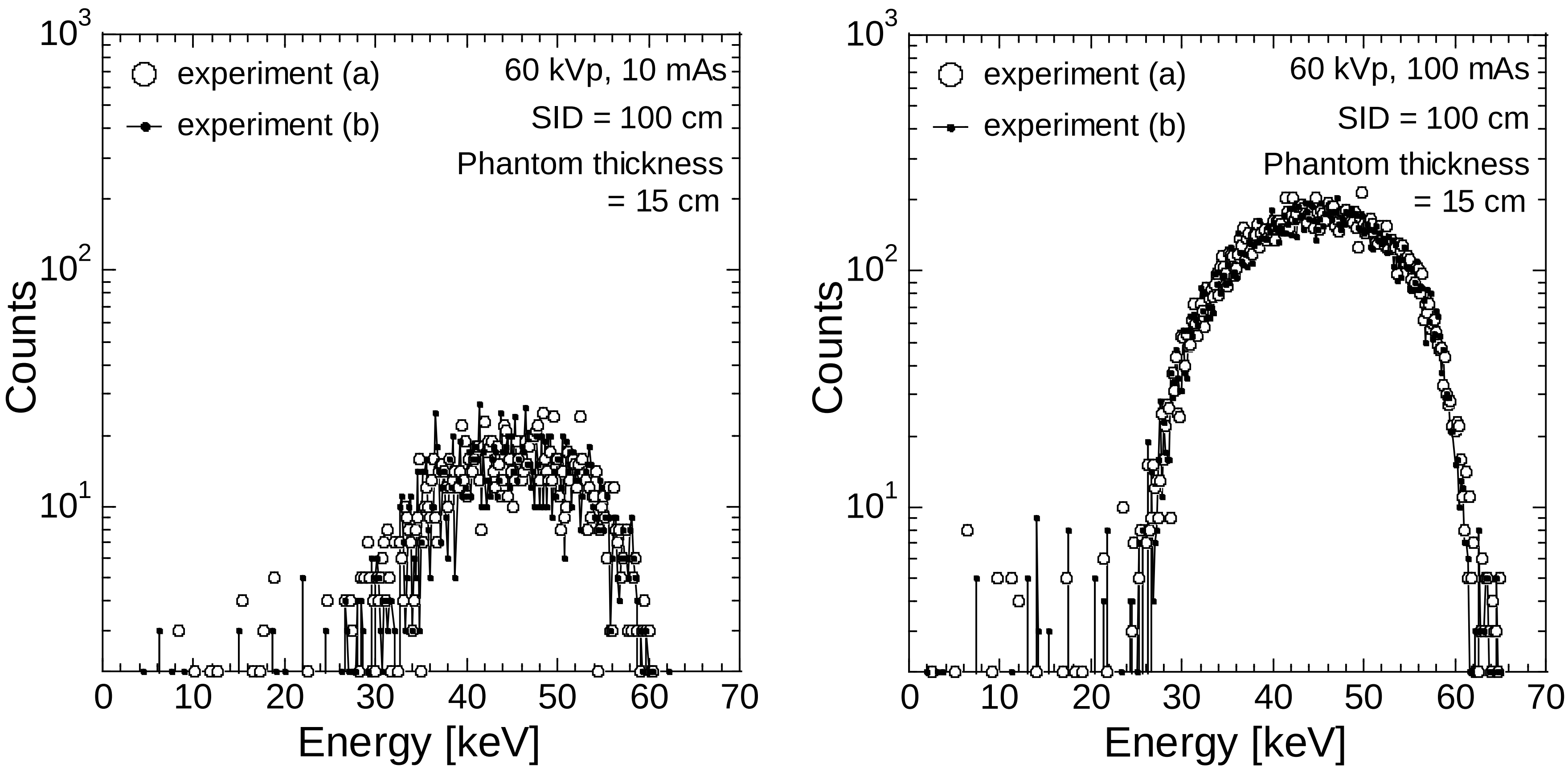

Fig.2

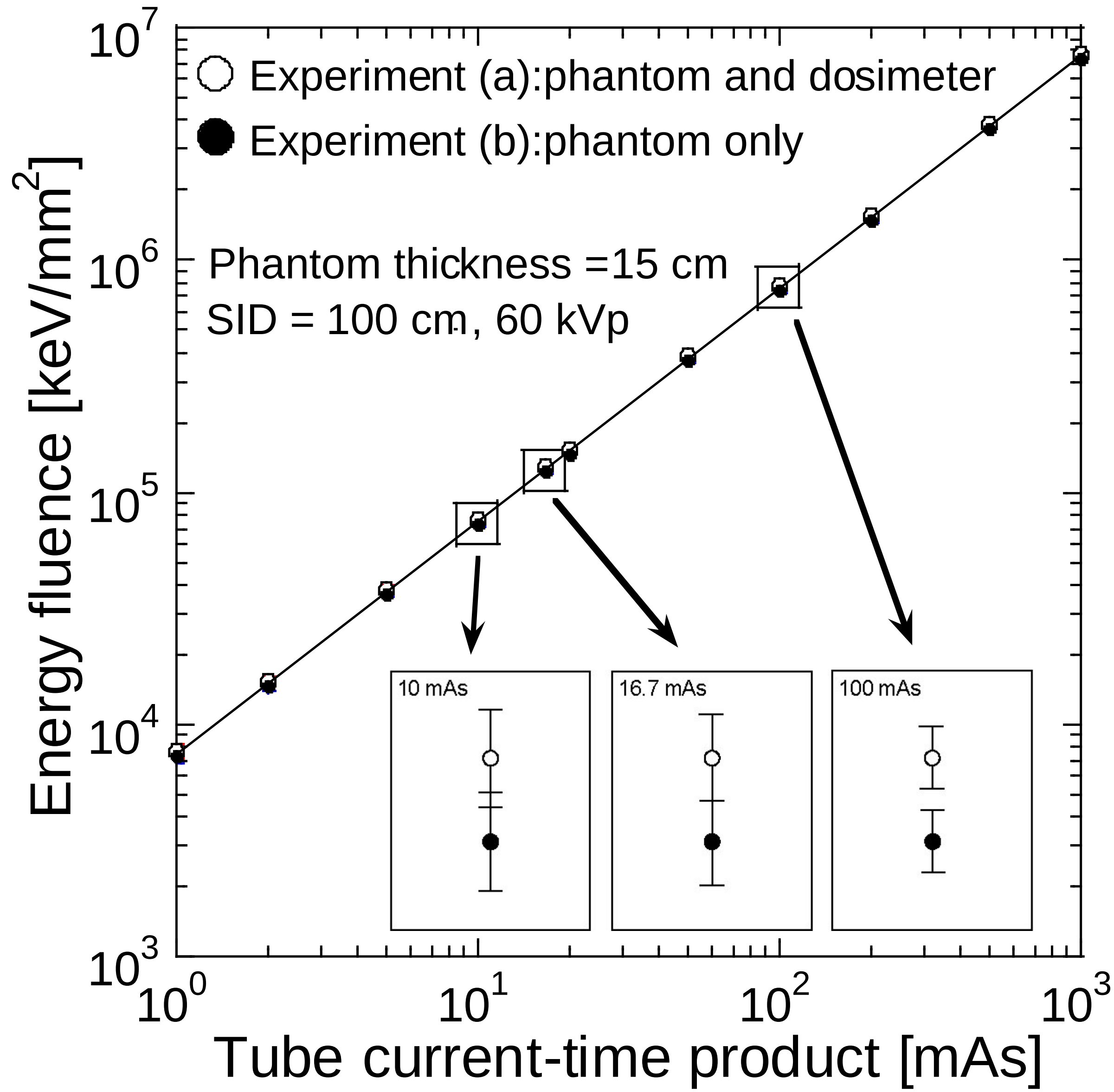

Experiment (a):phantom and dosimeter
Experiment (b):phantom only
Phantom thickness =15 cm
SID = 100 cm, 60 kVp
10 mAs
16.7 mAs
100 mAs
Energy fluence [keV/mm^2]
Tube current-time product [mAs]
10^3
10^4
10^5
10^6
10^7
10^0
10^1
10^2
10^3

Fig.3

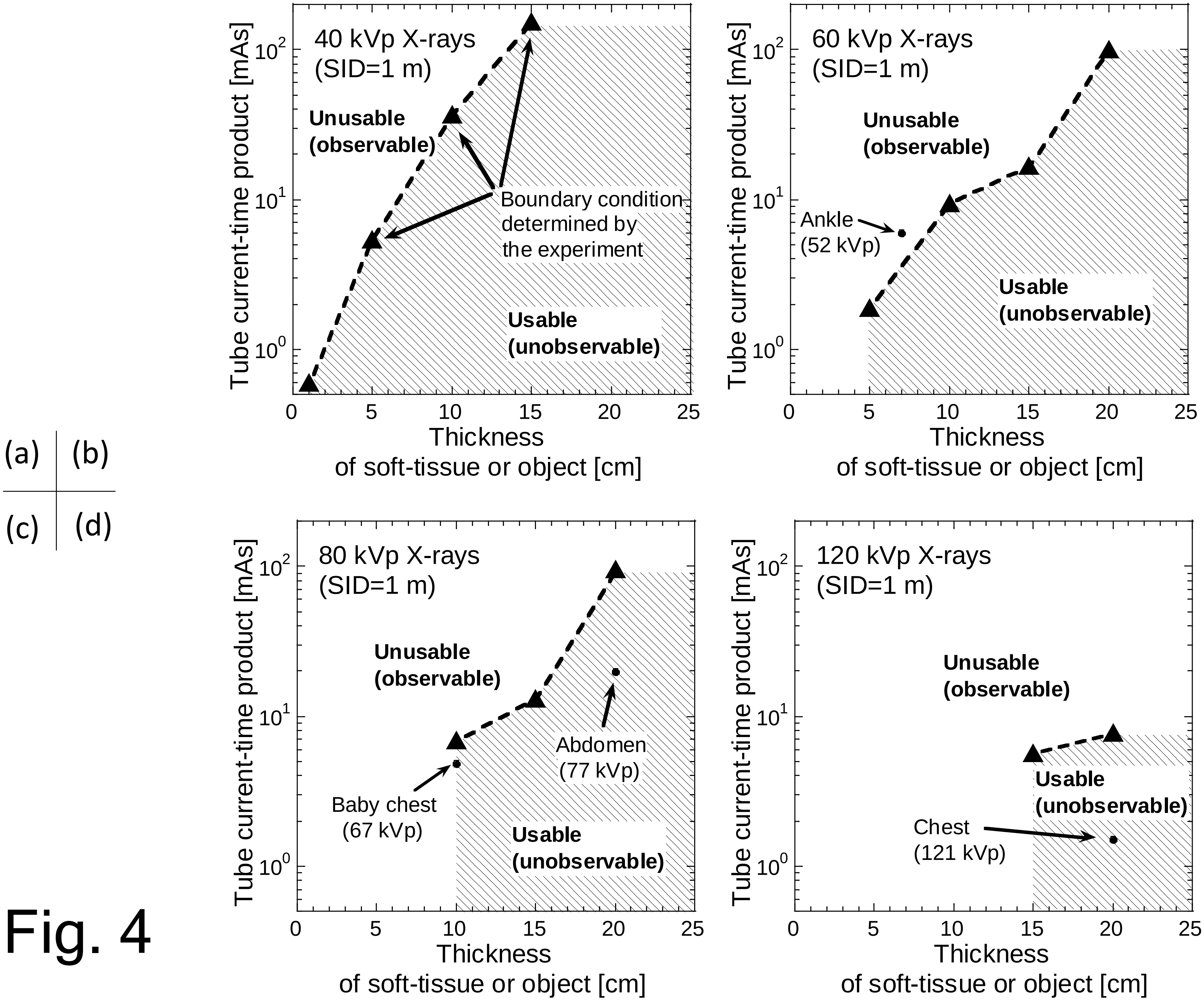

40 kVp X-rays
(SID=1 m)
Unusable
(observable)
Boundary condition
determined by
the experiment
Usable
(unobservable)
Tube current-time product [mAs]
Thickness
of soft-tissue or object [cm]
60 kVp X-rays
(SID=1 m)
Unusable
(observable)
Ankle
(52 kVp)
Usable
(unobservable)
Tube current-time product [mAs]
Thickness
of soft-tissue or object [cm]
80 kVp X-rays
(SID=1 m)
Unusable
(observable)
Abdomen
(77 kVp)
Baby chest
(67 kVp)
Usable
(unobservable)
Tube current-time product [mAs]
Thickness
of soft-tissue or object [cm]
120 kVp X-rays
(SID=1 m)
Unusable
(observable)
Usable
(unobservable)
Chest
(121 kVp)
Tube current-time product [mAs]
Thickness
of soft-tissue or object [cm]
(a) (b)
(c) (d)

Fig. 4

Table 1 Irradiation conditions used

Tube voltage[kV]	Phantom thickness[cm]	Current-time products[mAs]
40	1	0.5-50
	5	0.5-50
	10	2-200
	20	20-1000
60	5	0.5-20
	10	1-50
	15	5-200
	20	20-500
80	10	0.5-20
	15	2-50
	20	5-200
120	15	0.5-20
	20	1-50

Table 2 Summary of boundary conditions

Phantom thickness [cm]	tube current-time product [mAs] concerning the irradiation dose			
	40 kV	60 kV	80 kV	120 kV
1	0.6	-	-	-
5	5.4	1.9	-	-
10	36.9	9.4	6.9	-
15	154.7	16.7	13.1	5.7
20	-	100.4	95.6	7.8